44th AIAA/ASME/SAE/ASEE Joint Propulsion Conference & Exhibit
21 - 23 July 2008, Hartford, CT

AIAA 2008-4834

On the Compressible Bidirectional Vortex

Brian A. Maicke* and Joseph Majdalani†

University of Tennessee Space Institute, Tullahoma, TN 37388

The purpose of this paper is to develop a theoretical solution that describes the compressible bidirectional vortex. Similar studies by the authors have extended the Taylor and Culick profiles to incorporate the effects of compressibility in porous channels and tubes. Our study is prompted by the need to better understand the flow behavior at high speed in swirl-driven thrust chambers in which a reversing cyclonic motion is established. Such chambers have the advantage of promoting mixing, efficiency, and internal wall cooling. This is accomplished by confining combustion to an inner vortex tube that remains separated from the chamber walls by an outer stream of swirling, low temperature oxidizer. Our closed-form analytical solution is based on steady, rotational, axisymmetric, compressible, and inviscid flow conditions. It is constructed using a Rayleigh-Janzen expansion in the injection Mach number. At the outset, the compressible axial and radial velocities are captured along with the mantle movement at various Mach numbers and vortex Reynolds numbers. In view of the underlying assumption of axisymmetry, all properties are held constant about the chamber axis. We find that, so long as this condition is maintained, the swirl velocity remains invariant in the tangential direction.

Nomenclature

a	= chamber radius
a_0	= speed of sound
A_i	= inlet area
b	= chamber outlet radius
L	= chamber aspect ratio, L_0 / a
L_0	= chamber aspect ratio, L_0 / a
M_i	= injection Mach number, U / a_0
p	= normalized pressure, $\overline{p} / p_0$
$\overline{Q}_i$	= inlet volumetric flow rate
Q_i	= normalized volumetric flow rate in, $\overline{Q}_i / (Ua^2) = \sigma^{-1}$
Re	= injection Reynolds number, $Ua / \nu = 1 / \varepsilon$
r	= normalized radial coordinate, $\overline{r} / a$
S	= swirl number, $\pi ab / A_i = \pi\beta\sigma$
$\boldsymbol{u}$	= normalized velocity $(\overline{u}, \overline{v}, \overline{w}) / U$
u_θ	= normalized swirl/spin/tangential velocity, $\overline{u}_\theta / U$
U	= mean inflow velocity, $\overline{u}_\theta(a, L)$
V	= vortex Reynolds number, $Q_i Re(a / L) = (\varepsilon\sigma l)^{-1}$
z	= normalized axial coordinate, $\overline{z} / a$

*Doctoral Research Assistant, Department of Mechanical, Aerospace and Biomedical Engineering. Member AIAA.

†H. H. Arnold Chair of Excellence in Advanced Propulsion, Department of Mechanical, Aerospace and Biomedical Engineering. Member AIAA. Fellow ASME.

Greek

β = normalized outlet radius, b / a
ε = perturbation parameter, $1 / Re = \nu / (Ua)$
κ = inflow parameter, $Q_i / (2\pi l) = (2\pi\sigma l)^{-1}$
ν = kinematic viscosity, μ / ρ
ρ = density
σ = modified swirl number, $Q_i^{-1} = S / (\pi\beta)$

Subscripts and Symbols

i = inlet property
r = radial component or partial derivative
z = axial component or partial derivative
$\underline{\theta}$ = azimuthal component or partial derivative
= overbars denote dimensional variables

I. Introduction

THE theory of rotating flows continues to attract attention in a multitude of research areas because of its rich attributes, daunting complexity, and scalability benefits. Traditionally, the application of swirl is extensively used as a vehicle for efficient and stable combustion in industrial furnaces, utility boilers, spiraling heat exchangers, gas turbines with toroidal zones, turbofans with swirl augmenters, etc. It is heavily used in the dust separation industry[1-3] and has recently coursed its way to the propulsion community.[4-7] Of particular interest to us are cyclonic flows that exhibit a bidirectional coaxial motion that is neither triggered by vortex breakdown nor instability.[8,9] Such flows are also characterized by the formation of a non-translating layer separating the upward and downward fluid streams. This spinning interfacial layer is often termed *mantle* and the spiraling streams are dubbed the outer and inner vortices (see Fig. 1).

One of the earliest investigations of cyclonic motions in dust separators may be traced back to ter Linden.[10] In subsequent years, a simple analytical model for the incompressible flow in a conical cyclone was obtained by Bloor and Ingham.[11] CFD simulations followed by Hsieh and Rajamani,[12] Hoekstra Derksen and Van den Akker,[13] Derksen and Van den Akker,[14] and others. Hoekstra and co-workers also conducted laboratory tests using Laser-Doppler Velocimetry (LDV) to verify their numerical simulations of

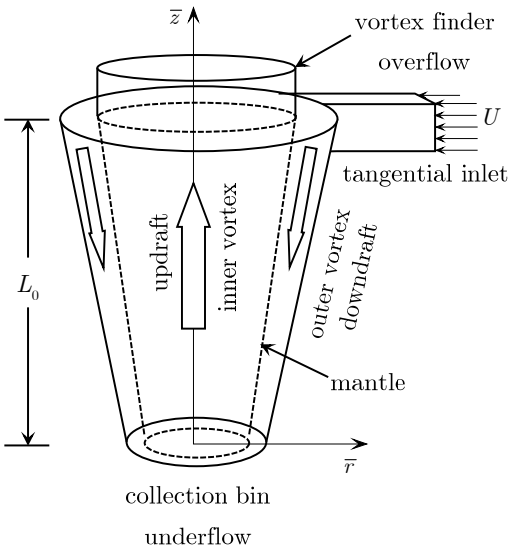

Figure 1. Sketch of a cyclonic separator.

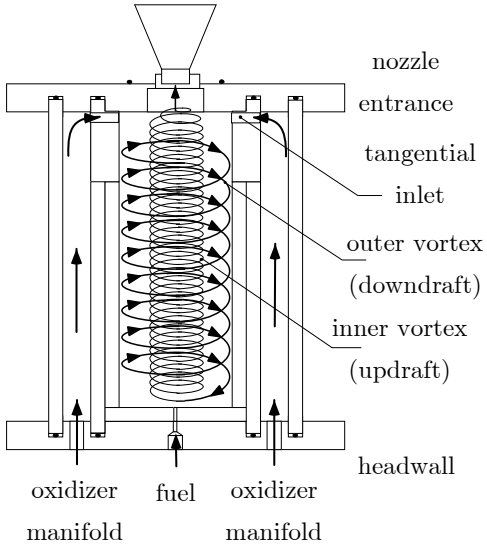

Figure 2. Sketch of a wall-cooled vortex engine.

this problem. However, no investigation has yet focused on the compressible flow aspects of bidirectional vortices.

Our particular interest in cyclonic motions serves two main objectives: to enhance our modeling capabilities of cyclone separators, and to better understand the factors that influence the gaseous motion in vortex-fired liquid rocket engines. Of the two settings, it is the propulsive thrust that constitutes the principal motivation for this study. In this vein, trapping the energy of a cyclone inside a combustor has been recently exploited in several noteworthy programs. These include the Vortex Combustion Cold-Wall Chamber (VCCWC) by Chiaverini *et al.,*[4] the Vortex Fired Hybrid Engine by Gloyer, Knuth and Goodman,[5] the Vortex Injection Hybrid Rocket Engine (VIHRE) by Knuth *et al.*,[6] and the Reverse Vortex Combustor (RVC) by Matveev *et al.*[7]

So while interest in improving industrial cyclones continues to rise in countries affected by pollution, the implementation of a fully reversing bidirectional swirl has justified the development of lightweight combustion devices often referred to as Vortex Engines. One such example consists of a Vortex Combustion Cold-Wall Chamber, an unconventional thrust chamber in which the oxidizer is injected just upstream of the nozzle entrance and tangentially to the inner walls (see Fig. 2).[4] After entering the chamber at the base, the oxidizer spirals toward the headwall where fuel is added. The entrained oxidizer-fuel mixture then reverses and spirals inwardly, accelerating as it enters the nozzle. The reversed flow is characterized by higher velocities to the extent of necessitating a compressible flow treatment.

As in cyclones, a non-translating mantle separates the outer updraft from the inner downdraft, thus confining combustion products to the inner vortex region. The inner swirl increases fuel residence time, turbulence, and propellant mixing, thus improving the overall thrust and reducing the chamber length needed to achieve a desired performance level. The outer vortex protects the chamber walls from excessive heating loads to the extent of not only reducing cooling requirements, but also permitting more flexibility in material selection.

Assuming incompressible flow conditions, mathematical representations of the bidirectional vortex have been developed by Vyas and Majdalani,[15] Majdalani and Rienstra,[16] and Vyas, Majdalani and Chiaverini[17-19] for the VCCWC liquid engine application. For the hybrid engine case, a closed-form solution has been advanced by Majdalani.[20] Cold flow experimentation using PIV[21,22] and numerical models have been performed in parallel under both cold[23] and reactive flow conditions.[24]

In order to devise a mathematical framework for the compressible bidirectional vortex, one may either adopt an integral approach after Balakrishnan, Liñan, and Williams[25,26] or pursue a Rayleigh-Janzen expansion after Majdalani[27] or Maicke and Majdalani.[28] These studies are specialized in describing the compressibility effects that impact the core flow in solid propellant rocket motors. In this study, we choose the Rayleigh-Janzen technique in conjunction with the original bidirectional vortex established in an axisymmetric, constant-diameter chamber with tangential wall injection. In the process, we expand the system of equations up to fourth order in the injection Mach number.

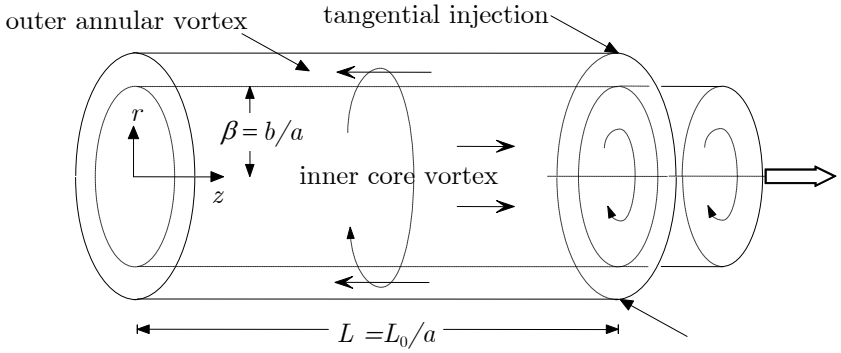

Figure 3. Geometric characteristics of the bidirectional vortex chamber.

II. Mathematical Model

A. Geometry

Our work focuses on the inviscid, axisymmetric, compressible, steady, rotational flow inside a cylindrical chamber of length L_0 and radius a, shown schematically in Fig. 3. The origin of the coordinate system is fixed at the center of the inert headwall, and a partially open downstream end is taken to have a radius b. The radial and axial directions are denoted by $\overline{r}$ and $\overline{z}$, respectively. A single phase, non-chemically reactive fluid is injected at the base of the chamber, at $\overline{r} = a$, in a purely tangential manner and at an average circumferential velocity of $\overline{v} = U$. The injected fluid quickly develops axial motion that drives the fluid upwardly in a helical manner. Upon reaching the headwall, the flow reverses axial direction and spirals down the center of the chamber, exiting at $\overline{z} = L_0$. The defining geometric parameters consist of the aspect ratio of the chamber, given by $L = L_0 / a$, and the fraction of radius open at the base, defined as $\beta = b / a$.

It may be instructive to note that unlike cyclonic flows that possess dual outlets, the bidirectional coaxial field observed in the liquid propellant thrust chamber has only one outlet section. In order to better understand its formation and stability to spatial and periodic disturbances; it would be of great benefit if particularly simple forms for the velocity and pressure components could be obtained. For this reason, it is the purpose of this study to provide closed-form approximations that can be used to describe the compressible gas motion in this particular swirl-driven liquid propellant thrust chamber.

B. Basic Formulation

We begin our analysis by adopting the following normalization scheme

$$\begin{cases} r = \dfrac{\overline{r}}{a}; \quad z = \dfrac{\overline{z}}{a}; \\ u = \dfrac{\overline{u}}{U}; \quad v = \dfrac{\overline{v}}{U}; \quad w = \dfrac{\overline{w}}{U}; \\ \Omega = \dfrac{\overline{\Omega} a}{U}; \quad \psi = \dfrac{\overline{\psi}}{U \rho_0 a^2} \\ p = \dfrac{\overline{p}}{p_0}; \quad T = \dfrac{\overline{T}}{T_0}; \quad \rho = \dfrac{\overline{\rho}}{\rho_0}; \quad Q_i = \dfrac{\overline{Q}_i}{U a^2}; \quad \nabla = a\overline{\nabla} \end{cases} \tag{1}$$

When these relations are applied to the axisymmetric governing equations we find that conservation of mass becomes

$$u\frac{\partial \rho}{\partial r} + w\frac{\partial \rho}{\partial z} + \rho\left[\frac{1}{r}\frac{\partial (ru)}{\partial r} + \frac{\partial w}{\partial z}\right] = 0 \tag{2}$$

while radial, tangential and axial momentum conservations yield

$$u\frac{\partial u}{\partial r} - \frac{\partial v^2}{r} + w\frac{\partial u}{\partial z} = \frac{1}{\gamma \rho M_i^2}\frac{\partial p}{\partial r} \tag{3}$$

$$u\frac{\partial v}{\partial r} + \frac{uv}{r} = \frac{1}{Re}\frac{\partial}{\partial r}\left[\frac{1}{r}\frac{\partial (rv)}{\partial r}\right] \tag{4}$$

and

$$w\frac{\partial w}{\partial z} + u\frac{\partial w}{\partial r} = \frac{1}{\gamma \rho M_i^2}\frac{\partial p}{\partial z} \tag{5}$$

respectively. Finally, to bring closure to the thermodynamic properties we use the isentropic flow relations

$$\begin{cases} \rho = p^{1/\gamma} \\ T = p^{1-1/\gamma} \end{cases} \tag{6}$$

These equations are subject to the following boundary conditions

$$\begin{cases} \overline{r}=a, \overline{z}=L_0, \overline{v}=U & \text{circumferential velocity at entry} \\ \overline{r}=0, \forall \overline{z}, \overline{v}=0 & \text{forced vortex center} \\ \overline{z}=0, \forall \overline{r}, \overline{w}=0 & \text{impervious headwall} \\ \overline{r}=0, \forall \overline{z}, \overline{u}=0 & \text{no flow across centerline} \\ \overline{r}=a, \forall \overline{z}, \overline{u}=0 & \text{impervious sidewall} \\ \int_b^a \overline{w}(\overline{r}, L_0)\overline{r}\mathrm{d}\overline{r}=\overline{Q}_i & \text{axial inflow matching tangential source} \end{cases} \tag{7}$$

C. Rayleigh-Janzen Method

In order to apply the Rayleigh-Janzen method, one further simplification is required from the basic equations used in the previous section. Because we have decoupled the swirl component from the axial and radial velocities, we are able to simplify the model through the introduction of the Stokes stream function. This is related to the velocities and vorticity via

$$\begin{aligned} u &= -\frac{1}{\rho r}\frac{\partial \psi}{\partial z}; w = \frac{1}{\rho r}\frac{\partial \psi}{\partial r} \\ \Omega_\theta &= -\frac{1}{r}\frac{\partial}{\partial z}\left(\frac{1}{\rho}\frac{\partial \psi}{\partial z}\right) - \frac{\partial}{\partial r}\left(\frac{1}{\rho r}\frac{\partial \psi}{\partial r}\right) \end{aligned} \tag{8}$$

Next, we expand the terms in the vorticity equation to find

$$\mathrm{D}^2\psi + r\rho\Omega_\theta = \frac{1}{\rho}\nabla\rho\cdot\nabla\psi \tag{9}$$

where the Stokes operator emerges as

$$\mathrm{D}^2 \equiv \frac{\partial^2}{\partial r^2} - \frac{1}{r}\frac{\partial}{\partial r} + \frac{\partial^2}{\partial z} \tag{10}$$

In order to solve the newly introduced vorticity equation, another relationship must be established between the vorticity and the stream function. We bring closure to the system by invoking the vorticity transport equation

$$\nabla\times\left(\boldsymbol{U}\times\boldsymbol{\Omega}\right) = -\frac{1}{\gamma M_i^2\rho^2}\nabla\rho\times\nabla p \tag{11}$$

With the governing equations fully determined, we then apply a Rayleigh-Janzen perturbation of the Mach number squared. This expansion starts from:

$$\begin{aligned} u(r,z) &= u_0 + M_i^2 u_1 + O(M_i^4) & \rho(r,z) &= 1 + M_i^2\rho_1 + M_i^4\rho_2 + O(M_i^6) \\ v(r,z) &= v_0 + M_i^2 v_1 + O(M_i^4) & p(r,z) &= 1 + M_i^2 p_1 + M_i^4 p_2 + O(M_i^6) \\ \psi(r,z) &= \psi_0 + M_i^2\psi_1 + O(M_i^4) & T(r,z) &= 1 + M_i^2 T_1 + M_i^4 T_2 + O(M_i^6) \\ \Omega(r,z) &= \Omega_0 + M_i^2\Omega_1 + O(M_i^4) \end{aligned} \tag{12}$$

After segregating terms by order we find the leading and first order velocities to be connected to the stream function and density via

$$\begin{aligned} O(1): u_0 &= -\frac{1}{r}\frac{\partial\psi_0}{\partial z}; \quad w_0 = \frac{1}{r}\frac{\partial\psi_0}{\partial r} \\ O(M_i^2): u_1 &= \frac{\rho_1}{r}\frac{\partial\psi_0}{\partial z} - \frac{1}{r}\frac{\partial\psi_1}{\partial z}; \quad w_1 = \frac{1}{r}\frac{\partial\psi_0}{\partial r} - \frac{\rho_1}{r}\frac{\partial\psi_0}{r} \end{aligned} \tag{13}$$

On substitution into the governing equations at the leading order we find

$$\nabla\times(\boldsymbol{U}_0\times\boldsymbol{\Omega}_0) = 0 \tag{14}$$

$$\mathrm{D}^2\psi_0 + r\Omega_0 = 0 \tag{15}$$

$$\frac{\partial v_0}{\partial r} + \frac{v_0}{r} = 0 \tag{16}$$

$$-\frac{1}{\gamma}\frac{\partial p_1}{\partial r} = u_0\frac{\partial u_0}{\partial r} + w_0\frac{\partial u_0}{\partial z} - \frac{v_0^2}{r} \tag{17}$$

$$-\frac{1}{\gamma}\frac{\partial p_1}{\partial z} = w_0\frac{\partial w_0}{\partial z} + u_0\frac{\partial w_0}{\partial r} \tag{18}$$

$$\rho_1 = \frac{p_1}{\gamma}; \quad T_1 = \frac{\gamma-1}{\gamma}p_1 \tag{19}$$

When the boundary conditions of Eq. (7) are expanded, we obtain the leading order assortment

$$v_0(1,L)=1; \quad v_0(0,z)=0; \quad w_0(r,0)=0; \quad u_0(0,z)=0; \quad u_0(1,z)=0; \quad \int_0^\beta w_0(r,z)r\mathrm{d}r = Q_i \tag{20}$$

In a similar manner, we separate the first order equations to yield

$$\nabla\times(\boldsymbol{U}_0\times\boldsymbol{\Omega}_1) + \nabla\times(\boldsymbol{U}_1\times\boldsymbol{\Omega}_0) = -\frac{\nabla\rho_1\times\nabla p_1}{\gamma} \tag{21}$$

$$\mathrm{D}^2\psi_1 + r\Omega_1 = \nabla\rho_1\cdot\nabla\psi_0 - r\Omega_0\rho_1 \tag{22}$$

$$\frac{\partial v_1}{\partial r} + \frac{v_1}{r} = 0 \tag{23}$$

$$-\frac{1}{\gamma}\frac{\partial p_2}{\partial r} = \rho_1\left(u_0\frac{\partial u_0}{\partial r} + w_0\frac{\partial u_0}{\partial z} - \frac{v_0^2}{r}\right) + \frac{\partial(u_0u_1)}{\partial r} + w_0\frac{\partial(u_1)}{\partial z} + w_1\frac{\partial(u_0)}{\partial z} \tag{24}$$

$$-\frac{1}{\gamma}\frac{\partial p_2}{\partial z} = \rho_1\left(w_0\frac{\partial w_0}{\partial z} + u_0\frac{\partial w_0}{\partial r}\right) + \frac{\partial(w_0w_1)}{\partial z} + u_0\frac{\partial(w_1)}{\partial r} + u_1\frac{\partial(w_0)}{\partial r} \tag{25}$$

$$\rho_2 = \frac{p_2}{\gamma} + \frac{1-\gamma}{2\gamma^2}p_1^2; \quad T_2 = \frac{\gamma-1}{\gamma}p_2 + \frac{\gamma-1}{2\gamma^2}p_1^2 \tag{26}$$

Corresponding boundary conditions yield

$$u_1(0,z)=0; \quad u_1(1,z)=0; \quad \int_0^\beta [\rho_1 w_0(r,z) + w_1(r,z)]r\mathrm{d}r = 0 \tag{27}$$

Furthermore, we implement homogenous boundary conditions at the first order so as not to disrupt the leading order results.

III. Solution

A. Leading Order Solution

One of the advantages of the Rayleigh-Janzen method is that the leading order solution reproduces the incompressible model. Details of the incompressible solution can be found in the works of Vyas and Majdalani[15] and Vyas, Majdalani and Chiaverini.[17,18] A summarized reconstruction is presented here for the reader's convenience. First, the swirl velocity is found to be decoupled from the other velocity components and as such can be treated separately. Second, the vorticity transport equation is tackled to relate the vorticity to the stream function. The leading order vorticity equation is then solved to determine the stream function. Once the stream function is found, the pressure and by extension the density and temperature are extrapolated. The results of the leading order solution are hence:

$$\psi_0 = \kappa z\sin(\pi r^2); \quad u_0 = -\frac{\kappa}{r}\sin(\pi r^2); \quad v_0 = \frac{1}{r}\left(1-e^{-\frac{1}{4}Vr^2}\right); \quad w_0 = 2\pi\kappa z\cos(\pi r^2) \tag{28}$$

$$p_1 = -2\pi^2z^2\gamma\kappa^2 + \frac{\gamma}{4}\left\{\begin{array}{l} 2-2r^{-2}\left[1+e^{-\frac{1}{2}r^2V} - 2e^{-\frac{1}{4}r^2V} + \kappa^2\sin^2\left(\pi r^2\right)\right] \\ +V\left[\mathrm{Ei}\left(-\frac{1}{2}V\right) - \mathrm{Ei}\left(-\frac{1}{4}V\right) + \mathrm{Ei}\left(-\frac{1}{4}r^2V\right) - \mathrm{Ei}\left(-\frac{1}{2}r^2V\right)\right] \end{array}\right\} \tag{29}$$

The density and temperature at the leading order are simply the pressure scaled by the γ multipliers in Eq. (19).

B. First Order Vorticity Transport

The compressible corrections begin by determining the relationship between the first order vorticity and stream function. It is not enough to assume the same relationship as the leading order, namely that $\Omega_1 = \pi^2 r\psi_1$, as this solution does not satisfy the vorticity transport equation. Instead, we examine the vorticity transport relation and see that while the assumed form is not completely correct, it does simplify the equation. We posit the following relation

$$\Omega_1 = \pi^2 r\psi_1 + \Omega_{1c} \tag{30}$$

where Ω_{1c} is a corrective function that allows Ω_1 to satisfy the vorticity transport relation. Substituting this form back into Eq. (21) provides

$$\frac{\partial\psi_0}{\partial z}\left(\frac{\partial\Omega_{1c}}{\partial r} - \frac{\Omega_{1c}}{r}\right) - \frac{\partial\psi_0}{\partial r}\frac{\partial\Omega_{1c}}{\partial z} = 4\pi^2 r\psi_0\left(\frac{\partial\rho_1}{\partial r}\frac{\partial\psi_0}{\partial z} - \frac{\partial\rho_1}{\partial z}\frac{\partial\psi_0}{\partial r}\right) \tag{31}$$

which yields the corrective function

$$\Omega_{1c} = rf(\psi_0) + \frac{\pi^2 z\kappa\sin\left(\pi r^2\right)}{r}\begin{Bmatrix} 4e^{-\frac{1}{4}r^2V} - 2e^{-\frac{1}{2}r^2V} + r^2V\left[\mathrm{Ei}\left(-\frac{1}{4}r^2V\right) - \mathrm{Ei}\left(-\frac{1}{2}r^2V\right)\right] \\ -2\left\{1 + \left[4\pi^2 r^2 z^2 + \sin^2\left(\pi r^2\right)\right]\kappa^2\right\} \end{Bmatrix} \tag{32}$$

where $f(\psi_o)$ is a yet to be determined function that will be used to satisfy the vorticity equation.

C. First Order Vorticity Solution

Once Ω_1 is fully determined, we can apply the relationship from Eq. (32) to Eq. (22). To facilitate a solution, we assume

$$\psi_1 = z^3 G(r) + zH(r) \tag{33}$$

$$f(\psi_0) = A_1 z\sin(\pi r^2) + A_2 z^3\sin^3(\pi r^2) \tag{34}$$

The form of these relationships are deduced from previous experience[27,28] and from the structure of the vorticity equation. Using Eq. (33), the second order partial differential equation is broken down into two second order ordinary differential equations. These are

$$G'' - \frac{G'}{r} + 4\pi^2 r^2 G = \frac{3}{4}\mathrm{A}_2 r^2\sin\left(\pi r^2\right) - \frac{1}{4}\mathrm{A}_2 r^2\sin\left(3\pi r^2\right) + 16\pi^4 r^2\sin\left(\pi r^2\right)\kappa^3 \tag{35}$$

$$\begin{aligned} H'' - \frac{H'}{r} + 4\pi^2 r^2 H = {} & \frac{\pi\kappa^3\cos\left(3\pi r^2\right)}{2r^2} + 2\pi^2\kappa^3\sin\left(\pi r^2\right) + 2\pi^2\kappa^3\sin\left(3\pi r^2\right) - 4\pi^2\kappa\sin\left(\pi r^2\right) \\ & -\pi\kappa r^{-2}\left[\tfrac{1}{2}\kappa^2 + 2e^{-\frac{1}{4}r^2V}\left(e^{-\frac{1}{4}r^2V} - 2\right) + 2\right]\cos\left(\pi r^2\right) + 2\pi^2 r^2\kappa\sin\left(\pi r^2\right) \\ & -\pi^2 r^2\kappa V\left(\mathrm{Ei}\left(-\tfrac{1}{4}V\right) - \mathrm{Ei}\left(-\tfrac{1}{2}V\right) + 2\mathrm{Ei}\left(-\tfrac{1}{2}r^2V\right) - 2\mathrm{Ei}\left(-\tfrac{1}{4}r^2V\right)\right)\sin\left(\pi r^2\right) \\ & +4e^{-\frac{r^2V}{4}}\pi^2\kappa(2 - e^{-\frac{r^2V}{4}})\sin\left(\pi r^2\right) + 6G - \mathrm{A}_1 r^2\sin\left(\pi r^2\right) \end{aligned} \tag{36}$$

These two coupled ODEs are then solved in succession to determine the first order compressible correction to the stream function. The six constants are determined by applying the boundary conditions of Eq. (27). It should be noted that each boundary condition actually supplies two equations. This stems from the requirement that each boundary condition must be null for all values of z. After applying the boundary conditions we find the fully determined stream function expression, specifically

$$\psi_1 = -\frac{1}{3}\pi^2 z^3\kappa^3\left[\cos\left(2\pi r^2\right) - 1\right]\sin\left(\pi r^2\right) + \frac{1}{8}\pi z\kappa\left[\sin\left(\pi r^2\right)\left[-2\mathrm{Si}\left(2\pi r^2\right) + \mathrm{Si}\left(4\pi r^2\right) - \mathrm{Si}(2\pi) + 2\mathrm{Si}(\pi)\right]\kappa^2\right.$$

$$+\cos\left(\pi r^2\right)\left(4e^{-\frac{1}{4}r^2V}\left(2-e^{-\frac{1}{4}r^2V}\right)-\left(r^2-1\right)\left[\gamma\left(3\kappa^2-4\right)-4\right]+\kappa^2\left\{\left[2\mathrm{Ci}(2\pi)-\mathrm{Ci}(4\pi)\right]r^2+2\gamma\left(r^2-1\right)\right\}\right.$$
$$-2\left(Vr^2+2\right)\mathrm{Ei}\left(-\tfrac{1}{2}r^2V\right)+2(Vr^2+4)\mathrm{Ei}\left(-\tfrac{1}{4}r^2V\right)+\kappa^2\left[8\ln(2)\left(r^2-1\right)-2\mathrm{Ci}\left(2\pi r^2\right)+\mathrm{Ci}\left(4\pi r^2\right)\right]$$
$$\left.+2\left(\kappa^2-4\right)\ln(r)-\left(r^2-1\right)\left[\ln(256\pi)\kappa^2+\ln\left(\frac{4096}{V^4}\right)\right]\right)\Bigg] \tag{37}$$

IV. Results

A. Thermodynamic Properties

Because of the important role that they play in evaluating the compressible velocities, some of the thermodynamic variables are examined here. We start with Fig. 4(a) which shows the pressure curve corresponding to the axial test cases. We remark that the pressure begins at unity at the head end sidewall (i.e., corner), being constrained by the pressure boundary conditions. As we follow the curve toward the core region, we see that the pressure depreciates as it approaches the centerline; it then levels out to a constant value as it reaches the core. We find that elevating the Mach number or vortex Reynolds number produces similar results, with increasing values leading to a lower pressure at the center. The Mach number appears to be the dominant parameter, with its variations generating a much larger difference in core pressure. However, the effects of varying V increase at higher values of M_i and as such cannot be ignored. The influence of the vortex Reynolds number is confined to the core region, unlike the Mach number which affects a wider area of the domain. This behavior is expected as compressibility manifests itself throughout the entire flow field, whereas the vortex Reynolds number stems from of a viscous perturbation near the centerline. It should be noted that despite the pressure displaying some axial dependence, it remains very slight. This trend is not surprising given the strong swirl dominated formulation of the problem. We expect a minor axial gradient that supports the relatively slight axial velocities, as borne out by the axial pressure gradient equation, $\partial p \,/\, \partial z = -4M_i^2\pi^2\gamma\kappa^2 z$; this expression evaluates to approximately $-0.006\, z$ for a typical motor geometry, thus explaining its small relative contribution. The larger radial pressure gradients, shown in Fig. 4(b) drive the flow to the center of the chamber, closer to the core so that it may exit at the semi-open base. As M_i and V are increased, we see steeper gradients in the viscous core with the Mach number variations causing the largest changes and the vortex Reynolds number playing a lesser, but still non-negligible role. Outside of the mantle, the pressure and radial pressure gradient curves flatten out, reflecting a weaker sensitivity to the control parameters.

The density and pressure behave in a very similar manner to the pressure, as each term only varies from the pressure by a constant determined by γ. The density is the key modifier as it appears in the first order velocity terms in Eq. (13). The density starts at 1 at the wall, and then tapers down as it approaches the core, where it levels out to a fixed value. It undergoes this change more slowly than the pressure curve, being related to the pressure by $1\,/\,\gamma$. As compressibility is accounted for, the fluid

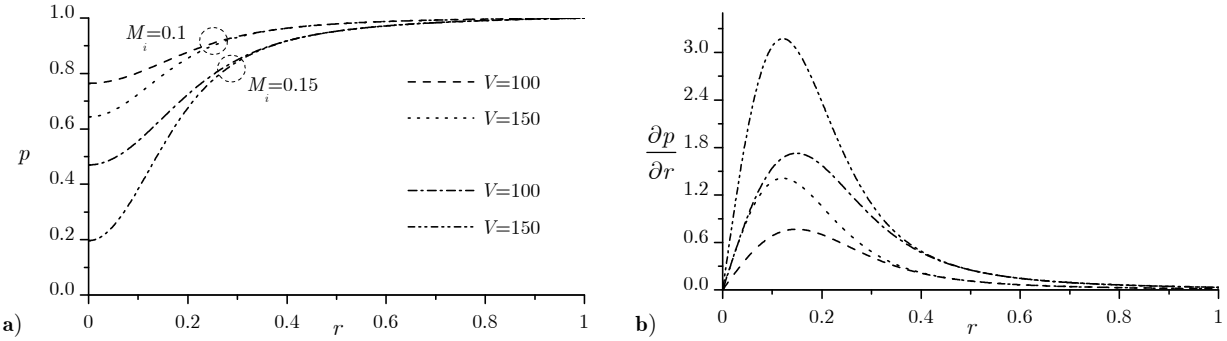

Figure 4. Pressure distribution and radial pressure gradient. Both parts use the same legend.

expands slightly as evidenced by the lower values of density. Conservation of mass requires the flow to increase in its axial velocity to account for this variation.

B. Velocity

We begin our velocity discussion with the tangential velocity. One would think that with the tangential velocity being the largest in magnitude of the velocities that it would be the most affected by compressibility effects. This is not the case. This observation has been backed experimentally by the observations of Mandella,[29] Cattafesta and Settles,[30] and Aboelkassem and Vastistas.[31] While these researchers were not specifically focused on the bidirectional vortex, their observation applies to a large number of vorticies, both confined and unbounded. This is valid analytically as well. One only needs to observe the absence of density affecting the swirl velocity in Eq. (23) and recognize that such behavior is a direct consequence of assuming axisymmetric flow. Unless axisymmetry is relaxed, the non-zero tangential pressure gradient in the azimuthal momentum equation precludes a compressible swirl velocity. While the swirl velocity itself is incompressible, it is the driving force behind the compressibility in the other velocities. The pressure, and by extension the density, is the dominant term in the radial momentum equation.

The axial velocity, pictured in Fig. 5(a), is calculated at a Mach number of 0.1, $\kappa = 0.1$ and $V = 200$. These values correspond to a realistic profile for the swirl velocity within a valid range of the perturbation expansion. Note that the velocity is plotted at three axial locations, namely $L = 0.25,\ 0.5$, and 0.75. As expected, we observe a slight increase in the velocity. At the location nearest to the headwall, the velocity increase is minor, as the flow has not had a chance to develop away from the headwall. As the flow nears the exit plane of the chamber, we see a more pronounced increase in the velocity. For the values considered here such behavior is physical, with a minute increase at the wall as the flow spirals toward the top of the chamber. However, as the flow reverses and makes it way down the center we see a larger increase in velocity. Thus as compressibility effects emerge, the density of the flow drops from its reference value at the wall. Then with fluid dilation, conservation of mass dictates that the flow must speed up to compensate for the change in density.

An interesting effect of compressibility is that the location of the mantle, the region where no axial translation takes place, is shifted toward the wall. The incompressible model has an analytical value of 0.707 for the geometry of the bidirectional vortex engine. This is predicated on the fraction of the radius open at the base, β, which is set at $\sqrt{2}/2$ for both studies. Compressibility seems to bring the location of the mantle closer to the values obtained by Smith[32] or Fang, Majdalani and Chiaverini.[23] For example, Smith has found an average radial fraction of 0.72 in his experimental work with cylindrical cyclone separators of a similar geometry. Fang, Majdalani and Chiaverini[23] found a value of 0.74. Table 1 shows the dependence of the mantle location with respect to the injection Mach number and the vortex Reynolds number. That the injection Mach number has the largest effect on the mantle location should be unsurprising as it is the key parameter for assessing compressibility effects. The vortex Reynolds number has a smaller effect. At our lowest value of Mach number, increasing the value of V only results in a change in the fourth decimal place of the fractional radius. For the $M_i = 0.2$ case, the effects of varying V are an order of magnitude larger. While, this is still minor compared to the dominance of the Mach number term, as the Mach number increases, the effect of the vortex Reynolds number must be accounted for. It should also be noted that with the advent of compressibility, the mantle location also displays a very weak dependence on κ and z. However, for the practical range of motor sizes, the variation in mantle location is so small as to be negligible.

Table 1 Compressibility effects on the mantle

M_i	V	Radial Fraction, β^*
0.05	75	0.7082
	125	0.7084
	200	0.7086
0.1	75	0.7113
	125	0.7121
	200	0.7129
0.15	75	0.7162
	125	0.7179
	200	0.7195
0.2	75	0.7224
	125	0.7253
	200	0.7278

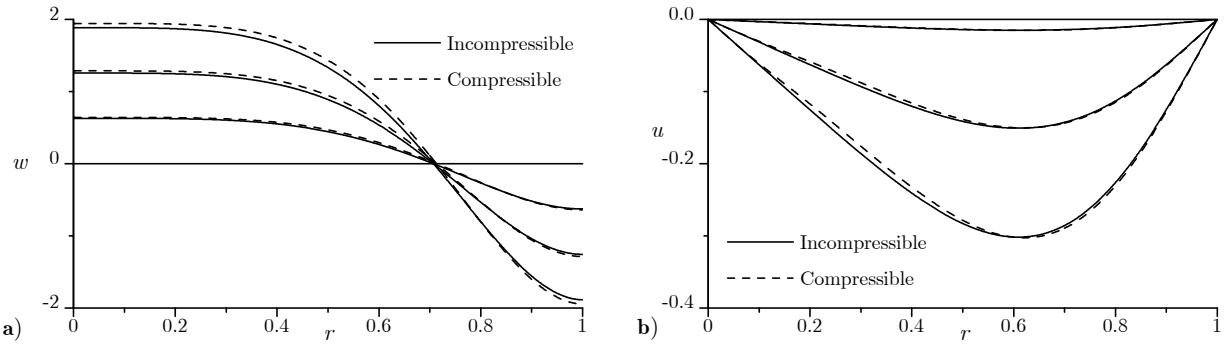

Figure 5. Axial and radial velocity comparisons.

The radial velocity depicted in Fig. 5(b) is calculated for the same parameters as the axial, with one exception. The values of κ are varied to values of $0.01, 0.1,$ and 0.2 to produce the three curves shown. Because the radial velocity is axially invariant, the graph shows how the radial velocity behaves as the chamber geometry is modified. As with the incompressible case, all radial velocities are inward, driven by the partially open chamber at the base. As the values of κ increase, so do the maxima exhibited by the radial velocity. When accounting for compressibility, the radial curve is shifted slightly to the right, producing an increased radial flow near the wall, and a small decrease in velocity closer to the core. Because there is no radial outflow, conservation of mass dictates that any increase in the outer region of the flow must be accompanied by a slowdown in the inner region. This is physically reasonable as we anticipate the outer flow to move towards the core more quickly; so as the flow approaches the centerline, it slows down as it enters the more congested core region where axial velocities are more dominant than the radial.

C. Vorticity

Because of its connection with the stream function expression at both the leading and first orders, it may be instructive to examine the vorticity behavior in the confined chamber and its sensitivity to the introduction of compressibility. Figure 6(a) quantifies the parametric effects of the compressible solution on the vorticity distribution. The curves are generated at $z = 2$ for a range of Mach numbers and vortex Reynolds numbers. As observed previously in the pressure comparison, the Mach number is the dominant agent in the compressible solution. However, even Mach number fluctuations have only a modest effect on the peak value of vorticity. It may be helpful to note that all of the azimuthal vorticity of the compressible profile appears in the outer free vortex region. We hence realize that the effect of the viscous perturbation near the centerline, which leads to a strong dependence on V, remains negligible. This behavior is delineated clearly when comparing vorticity profiles with variations in V for a constant Mach number. Compressibility introduces a nominal change in the vorticity distribution, as the compressible study displays less rotationality near the core. Moving outward past the radial midpoint, the compressible vorticity eclipses the incompressible prediction and maintains a higher value in the free vortex region until both models return to zero at the wall.

Figure 6(b) depicts the variance in vorticity for the axial locations $z = 1, 2,$ and 3. The compressible curves are calibrated with values of $M_i = 0.1$ and $V = 150$. We discover that as the axial distance increases, compressibility effects slowly increase. At the largest value of vorticity considered here, the difference between the compressible and incompressible vorticity peak is 0.55 or approximately 6.3% based on the incompressible value. Accounting for compressibility introduces a minor axial dependence to the peak vorticity location. For the incompressible case considered in Fig. 6(b), the peak location is approximately $r = 0.765$. The compressible counterparts start at $r = 0.767$ and progress to 0.766 and 0.764 for z values of $1, 2,$ and 3, respectively. This variation in the third decimal place reinforces our observation that for the typical short aspect ratio chambers associated with the bidirectional vortex engine, the rotationality of the flow is not significantly altered when compressibility effects are imposed.

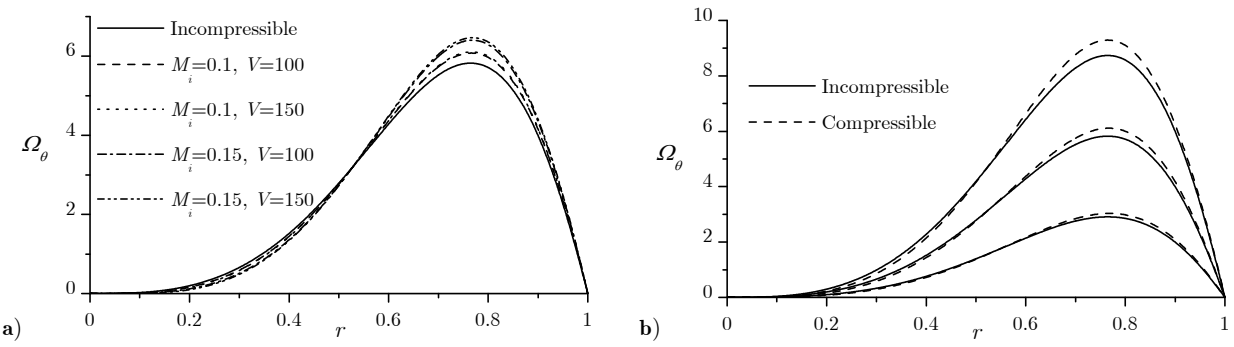

Figure 6. Compressibility effects on the azimuthal component of vorticity.

V. Conclusions

In this study, a compressible counterpart to the confined bidirectional vortex is introduced, using the Rayleigh-Janzen expansion to determine compressible corrections to the mean flow. The closed form nature of the model is ideal for the fast evaluation required for initial parametric studies and is perhaps the most significant result of this work. The model can be used as a baseline for additional studies of the confined vortex, such as hydrodynamic instability investigations. We are also able to isolate the effects of compressibility on the mantle location, which shifts the location of the mantle slightly outwardly from the core. This trend compares favorably with available experimental evidence.

The Rayleigh-Janzen method is not without its drawbacks. By its very nature, the present study requires small injection Mach numbers, so that the perturbation expansion remains sufficiently accurate. This is not normally a problem with confined flows, but there may be instances where the solution presented here begins to deteriorate as the injection Mach number is increased. In such an instance, retaining higher order terms would be required to maintain the fidelity of the solution. It is unlikely that such a higher order correction would be feasible in closed-form. The increase in intricacy from the leading order stream function to the first compressible correction show just how quickly the solution increases in complexity. It is likely that further compressible corrections may need to be captured numerically. When that point is reached the tradeoff between the Rayleigh-Janzen expansion and a full numerical solution to the Navier-Stokes equations would have to be revisited.

Even though the swirl velocity is found to be incompressible in this study, it has a great influence on the compressible corrections. A possible avenue for further study is to compare the effects of different swirl velocity models on the compressible corrections. Since the swirl velocity is separated from the axial and radial velocities, one may try available swirl velocity models that could suit the confined bidirectional vortex. Recently, Vatistas[33] and Maicke and Majdalani[34] have introduced alternate models for the swirl velocity of vortices. Classically, the works of Sullivan, Burgers, and Rankine could be re-examined as well. As compressibility effects are further explored, one could attempt to find a model that captures the swirl velocity accurately, but with less computational overhead. The result could be a compressible model that captures the important aspects observed here, but with less computational complexity.

Acknowledgments

This work has been supported partly by the National Science Foundation (CMMI-0353518) and partly by ORBITEC. The authors thank Dr. Martin J. Chiaverini, for his continuing support of this project.

References

[1]Peng, W., Hoffmann, A. C., and Dries, H., "Separation Characteristics of Swirl-Tube Dust Separators," *AIChE Journal,* Vol. 50, No. 1, 2004, pp. 87-96.

[2]Hu, L. Y., Zhou, L. X., Zhang, J., and Shi, M. X., "Studies of Strongly Swirling Flows in the Full Space of a Volute Cyclone Separator," *AIChE Journal,* Vol. 51, No. 3, 2005, pp. 740-749.

[3]Cortes, C., and Gil, A., "Modeling the Gas and Particle Flow inside Cyclone Separators," *Progress in Energy and Combustion Science,* Vol. in Press, 2007.

[4]Chiaverini, M. J., Malecki, M. J., Sauer, J. A., and Knuth, W. H., "Vortex Combustion Chamber Development for Future Liquid Rocket Engine Applications," AIAA Paper 2002-2149, July 2002.

[5]Gloyer, P. W., Knuth, W. H., and Goodman, J., "Overview of Initial Research into the Effects of Strong Vortex Flow on Hybrid Rocket Combustion and Performance," CSTAR Fifth Annual Symposium Paper N96- 16953, January 1993.

[6]Knuth, W. H., Chiaverini, M. J., Sauer, J. A., and Gramer, D. J., "Solid-Fuel Regression Rate Behavior of Vortex Hybrid Rocket Engines," *Journal of Propulsion and Power,* Vol. 18, No. 3, 2002, pp. 600-609.

[7]Matveev, I., Matveeva, S., and Serbin, S., "Design and Preliminary Test Results of the Plasma Assisted Tornado Combustor," AIAA Paper 2007-5628, July 2007.

[8]Smith, J. L., "An Analysis of the Vortex Flow in the Cyclone Separator," *Journal of Basic Engineering-Transactions of the ASME*, No. December, 1962, pp. 609-618.

[9]Smith, J. L., "An Experimental Study of the Vortex in the Cyclone Separator," *Journal of Basic Engineering-Transactions of the ASME*, No. December, 1962, pp. 602-608.

[10]ter Linden, A. J., "Investigations into Cyclone Dust Collectors," *Proceedings of the Institution of Mechanical Engineers,* Vol. 160, 1949, pp. 233-251.

[11]Bloor, M. I. G., and Ingham, D. B., "The Flow in Industrial Cyclones," *Journal of Fluid Mechanics,* Vol. 178, No. 1, 1987, pp. 507-519.

[12]Hsieh, K. T., and Rajamani, R. K., "Mathematical Model of the Hydrocyclone Based on Physics of Fluid Flow," *AIChE Journal,* Vol. 37, No. 5, 1991, pp. 735-746.

[13]Hoekstra, A. J., Derksen, J. J., and Van den Akker, H. E. A., "An Experimental and Numerical Study of Turbulent Swirling Flow in Gas Cyclones," *Chemical Engineering Science,* Vol. 54, No. 13, 1999, pp. 2055-2065.

[14]Derkson, J. J., and Van den Akker,H.E.A, "Simulation of Vortex Core Precession in a Reverse Flow Cyclone," *AIChE,* Vol. 46, No. 7, 2000, pp. 1317-1331.

[15]Vyas, A. B., and Majdalani, J., "Exact Solution of the Bidirectional Vortex," *AIAA Journal,* Vol. 44, No. 10, 2006, pp. 2208-2216.

[16]Majdalani, J., and Rienstra, S. W., "On the Bidirectional Vortex and Other Similarity Solutions in Spherical Coordinates," *Journal of Applied Mathematics and Physics (ZAMP),* Vol. 58, No. 2, 2007, pp. 289-308.

[17]Vyas, A. B., Majdalani, J., and Chiaverini, M. J., "The Bidirectional Vortex. Part 1: An Exact Inviscid Solution," AIAA Paper 2003-5052, July 2003.

[18]Vyas, A. B., Majdalani, J., and Chiaverini, M. J., "The Bidirectional Vortex. Part 2: Viscous Core Corrections," AIAA Paper 2003-5053, July 2003.

[19]Vyas, A. B., Majdalani, J., and Chiaverini, M. J., "The Bidirectional Vortex. Part 3: Multiple Solutions," AIAA Paper 2003-5054, July 2003.

[20]Majdalani, J., "Vortex Injection Hybrid Rockets," *Fundamentals of Hybrid Rocket Combustion and Propulsion*, edited by K. Kuo and M. J. Chiaverini, AIAA Progress in Astronautics and Aeronautics, Washington, DC, 2007, pp. 247-276.

[21]Anderson, M. H., Valenzuela, R., Rom, C. J., Bonazza, R., and Chiaverini, M. J., "Vortex Chamber Flow Field Characterization for Gelled Propellant Combustor Applications," AIAA Paper 2003-4474, July 2003.

[22]Rom, C. J., Anderson, M. H., and Chiaverini, M. J., "Cold Flow Analysis of a Vortex Chamber Engine for Gelled Propellant Combustor Applications," AIAA Paper 2004-3359, July 2004.

[23]Fang, D., Majdalani, J., and Chiaverini, M. J., "Simulation of the Cold-Wall Swirl Driven Combustion Chamber," AIAA Paper 2003-5055, July 2003.

[24]Fang, D., Majdalani, J., and Chiaverini, M. J., "Hot Flow Model of the Vortex Cold Wall Liquid Rocket," AIAA Paper 2004-3676, July 2004.

[25]Balakrishnan, G., Liñan, A., and Williams, F. A., "Rotational Inviscid Flow in Laterally Burning Solid Propellant Rocket Motors," *Journal of Propulsion and Power,* Vol. 8, No. 6, 1992, pp. 1167-1176.

[26]Balakrishnan, G., Liñan, A., and Williams, F. A., "Compressible Effects in Thin Channels with Injection," *AIAA Journal,* Vol. 29, No. 12, 1991, pp. 2149-2154.

[27]Majdalani, J., "On Steady Rotational High Speed Flows: The Compressible Taylor-Culick Profile," *Proceedings of the Royal Society, London, Series A,* Vol. 463, No. 2077, 2007, pp. 131-162.

[28]Maicke, B. A., and Majdalani, J., "On the Rotational Compressible Taylor Flow in Injection-Driven Porous Chambers," *Journal of Fluid Mechanics,* Vol. 603, No. 1, 2008, pp. 391-411.

[29]Mandella, M. J., "Experimental and Analytical Studies of Compressibile Vortices," Ph.D. Dissertation, Stanford University, 1987.

[30]Cattafesta, L. N., and Settles, G. S., "Experiments on Shock/Vortex Interaction," AIAA Paper 92-0315, 1992.

[31]Aboelkassem, Y., and Vatistas, G., "New Model for Compressible Vortices," *Journal of Fluids Engineering,* Vol. 129, No. 8, 2007, pp. 1073-1079.

[32]Smith, J. L., "An Analysis of the Vortex Flow in the Cyclone Separator," *Journal of Basic Engineering-Transactions of the ASME*, 1962, pp. 609-618.

[33]Vatistas, G. H., "New Model for Intense Self-Similar Vortices," *Journal of Propulsion and Power,* Vol. 14, No. 4, 1998, pp. 462-469.

[34]Maicke, B. A., and Majdalani, J., "Heuristic Representation of the Swirl Velocity in the Core of the Bidirectional Vortex," AIAA Paper 2007-4122, June 2007.